IEEE Access
Multidisciplinary | Rapid Review | Open Access Journal

Received April 11, 2020, accepted April 24, 2020, date of publication May 6, 2020, date of current version May 19, 2020.

Digital Object Identifier 10.1109/ACCESS.2020.2992653

Wideband Low-Profile Luneburg Lens Based on a Glide-Symmetric Metasurface

FANGFANG FAN, (Member, IEEE), MINGBO CAI, JIACHEN ZHANG, ZEHONG YAN, AND JINXIAO WU

National Key Laboratory of Antennas and Microwave Technology, Xidian University, Xi'an 710071, China

Corresponding author: Fangfang Fan (fffan@mail.xidian.edu.cn)

ABSTRACT This paper presents a two-dimensional low-profile Luneburg lens that is designed by using a glide-symmetric metasurface. The entire lens consists of two mirrored metal plates with periodic metal pins, and the pins on one plate are glided exactly a half period of the unit cell compared with the pins on the other plate. The proposed design has not only a stable refractive index over a wide operating band but also no dielectric loss compared to other metamaterial-based lenses. In addition, it is easy to manufacture and can also largely reduce the production cost. The complete Luneburg lens is simulated in CST Microwave Studio, and the results demonstrate that the lens can work within 14 GHz–22 GHz, which is greater than 44% of the bandwidth. The measured results show that the lens also agrees well with the simulated lens. This lens antenna would be an excellent candidate for satellite communication applications.

INDEX TERMS Wideband, Luneburg lens, metasurface, glide-symmetric, half-height pins.

I. INTRODUCTION

In the millimeter wave band, antennas applied in satellite communication are subjected to very challenging specifications. To achieve long distance transmission, an antenna is usually required to achieve a high gain, and wideband performance, low cost and light weight are also important. To date, there have been various gain-enhancement approaches used for antennas, each with its advantages and disadvantages. For example, reflectors [1] have shown good performance not only with regards to the gain but also with regards to the wideband applications and ease of manufacture. However, they suffer from a large size and low aperture efficiency. Planar antenna arrays have been widely used in microstrip antennas and arrays [2]–[4], horn arrays [5], waveguide slot arrays [6], substrate-integrated waveguide (SIW)-based planar arrays [7], and the antenna arrays using gap waveguide technology [8]. These kinds of antennas are suitable for the communication systems that require high gain, but the feed network is more complex. Planar lens antennas are a good choice for applications requiring a high gain and low profile, and they have been widely used in the mmW-band.

The traditional implementation techniques of lens antennas are based on dielectric [9] or gradient index (GRIN) media [10], [11]. However, GRIN material does not exist naturally, and an artificial material is usually employed to play the role of GRIN media. According to the equivalent medium theory [12], the materials made from mixing materials with different electromagnetic properties in different proportions can achieve arbitrary permittivity. By properly selecting the unit cell, the desired equivalent permittivity and permeability can be obtained. Usually for the convenience of processing, we use a dielectric with holes [13] and dielectric pillars [14] to achieve a GRIN lens antenna, but in the mmW-band, the GRIN lens is difficult to fabricate with a large number of small and dense units.

Metamaterials have provided new opportunities to improve the radiation properties and ease the fabrication of conventional antennas, especially quasi-optical devices such as the Luneburg lens. Recently, a lens printed on a dielectric substrate inside a parallel-plate-waveguide (PPW) has been realized, which uses low-cost and simple PCB techniques [15]. The equivalent permittivity is mainly controlled by the shapes and physical dimensions of the printed patches, such as complementary closed ring (CCR) resonators [16], I-shaped [17] unit cells, printed circular patches [18] or transmission lines [19]. We can see that the losses increase with increasing frequencies with the existence of dielectrics. The printed metasurfaces limit the bandwidth because of introducing the TE mode. The complexity of the feed or radiating

The associate editor coordinating the review of this manuscript and approving it for publication was Davide Comite.

systems makes the design, integration and manufacturing of the antenna difficult.

To avoid the dielectric losses, a new lens antenna was recently proposed that is based on a variable PPW Fakir bed of nails and fed by an open-ended WR-51 standard waveguide. The antenna works from 10 GHz to 15 GHz and has a band width of 40% [20]. Glide symmetry for a one-dimensional periodic structure was first analyzed in the 1960s and 1970s [21]–[23]. Recently, there has been notable progress made on two-dimensional glide-symmetric metasurfaces [24]–[28], and in [24], [25], the glide symmetry was used to design effective waveguides and device in gap waveguide technology. In [26], an ultrawideband metasurface Luneburg lens was proposed, but there was no fabricated lens to test the analysis results. In [27], a fully-metallic Luneburg lens at the Ka band was presented with a bandwidth of 29%. A method to realize anisotropic two-dimensional designs with wideband operation was presented in [28], and a 30% compressed Luneburg lens from 1 GHz to 13 GHz can also be obtained.

In this paper, we present a wideband lens antenna based on glide-symmetric half-height pins embedded in the two mirrored metal plates. Benefiting from the characteristics of the gap waveguide, the two metal plates do not need to be connected, and the whole antenna can be manufactured with computer numerical control (CNC) technology which can reduce the production costs. CST Microwave Studio simulations demonstrate that the lens performs well as designed from 14 GHz to 22 GHz. Preliminary work and simulation results are shown in the literature [29]. Based on the previous work, we added three rows of electromagnetic bandgap (EBG) units of half-height pins to further reduce the back lobe. Finally, we use the WR-51 standard waveguide as the feed source, and a prototype lens antenna is fabricated. The measured results demonstrate good performance from 14 GHz to 22 GHz with a stable radiation pattern.

II. ANALYSIS OF THE UNIT CELL

The half-height pin, located on both sides of two mirrored metal plates with an air gap, is shown in Fig. 1(a). The selected parameters are the period of the unit cell p, width of the pin a, air gap g and height of the pin h, respectively. From the dispersion diagrams in Fig. 1(a), we can see that this structure has the same stop-band characteristics as the full-height pin in the gap waveguide [30], and no electromagnetic waves can propagate through this pin structure in the stop-band. As one of the EBG structures, a half-height pin was recently proposed in the literature [31]. Literature [32] also analyzed different versions of periodic structures made with metallic pins located inside a PPW. We can use the structure in [31] to inhibit the propagation of electromagnetic waves or add some guiding configurations to guide the transmission of electromagnetic waves, such as ridges in ridge gap waveguides [33], grooves in groove gap waveguides [34], or microstrip lines in inverted microstrip line gap waveguides [35]. Furthermore, the height of the pin can be reduced

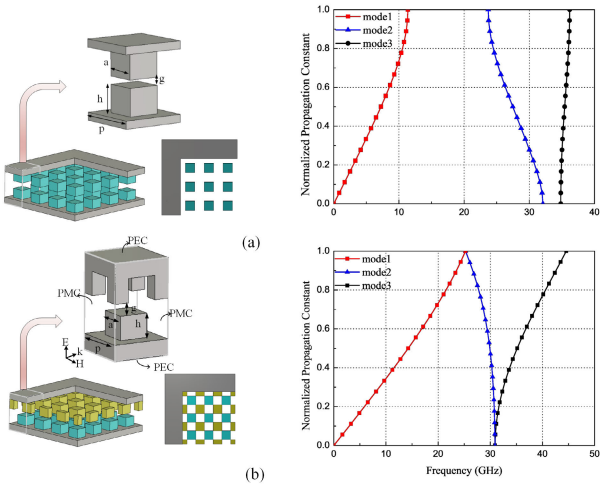

FIGURE 1. (a) The geometry of the symmetrical half-height pins. The dispersion diagram of the unit cell for the following dimensions: p = 8 mm, a = 4 mm, g = 0.52 mm and h = 1 mm. (b) The geometry of the glide symmetrical half-height pins. The dispersion diagram of the unit cell for the following dimensions: p = 4 mm, a = 2 mm, g = 1.52 mm and h = 1 mm.

by half to lower the fabrication cost compared with a full-height pin while retaining the stop-band characteristic.

When the two pin plates are glided, the unit cell shows different stop-band characteristics. Similar to the dispersion diagrams in the literature [31], the stop-band decreases with increasing glide distance. Herein, the proposed antenna is simulated and studied. When the symmetrical half-height pins glide exactly a half period of the unit cell, the geometry of the unit cell and dispersion diagram are shown in the inset of Fig. 1(b). We can see that the stop-band disappeared, and thus, electromagnetic waves can propagate through this structure in a wide band. Most importantly, the curve of the first mode becomes almost straight over a wide range of frequencies, thus demonstrating that this mode is essentially nondispersive. Therefore, this unit cell is an appropriate candidate for realizing a wideband lens antenna.

As shown in Fig. 1(b), the unit cell is excited by the plane wave, the direction of the electric field polarization is perpendicular to the two plates, and the directions of the electric field E, magnetic field H and wave propagation k have been given in Fig. 1(b). During the simulation of the dispersion diagram, the top and bottom sides of the unit cell are set as PEC, and the right and left sides of the unit cell are set as PMC. The electromagnetic properties of the unit cell can be determined exactly by solving Maxwell·s equations with a high-frequency structure simulator (HFSS). By extracting the amplitudes and phases of the waves reflected and transmitted from the unit cell, we can retrieve the permittivity and permeability values. Here, we adopt the S-parameter-based retrieval [36] to obtain the effective refractive index n.

$$n = \frac{1}{kd} cos^{-1}[\frac{1}{2S_{21}}(1 - S_{11}^2 + S_{21}^2)]. \tag{1}$$

$$z = \sqrt{\frac{(1 + S_{11})^2 - S_{21}^2}{(1 - S_{11})^2 - S_{21}^2}}. \tag{2}$$

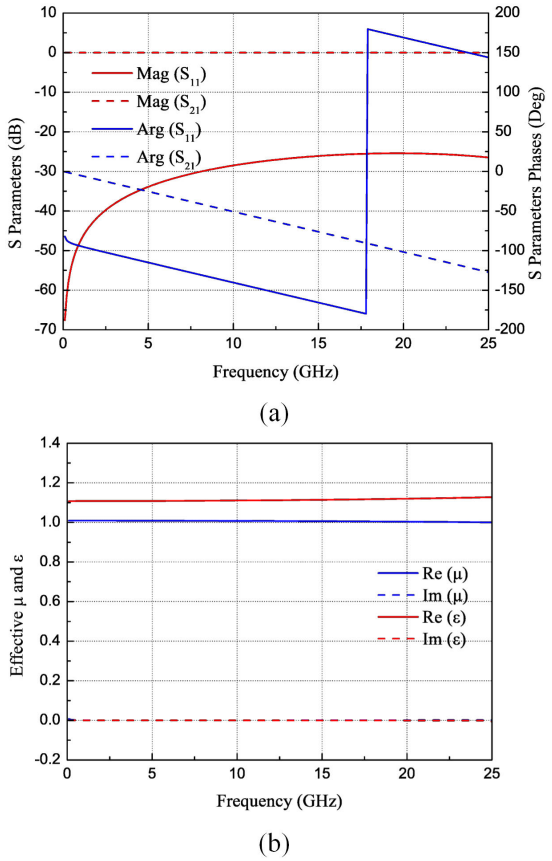

FIGURE 2. (a) Magnitude (red color) and phase response (blue color) of the scattering parameters for $h = 0.5$ mm. (b) Effective permittivity and permeability of the unit cell for $h = 0.5$ mm. The unit cell has the following dimensions: $p = 4$ mm, $a = 2$ mm and $g = 1.52$ mm.

where k represents the wavenumber, d is the period of the unit cell, and z is the wave impedance of the unit. n and z are related to μ and ϵ by the following relations

$$\epsilon = n/z, \mu = nz. \tag{3}$$

Fig. 2(a) illustrates the S-parameter with varied frequencies obtained by choosing $h = 0.5$ mm. The effective permittivity ϵ and permeability μ data are also plotted, as depicted in Fig. 2(b). By changing one or several parameters among the unit period p, pin size a, height h and air gap g, the refractive index of the unit cell can be changed as a function of the frequency. Here, we keep the parameters p, a and g constant, and the only parameter that is modified is the height of the pin h. The curve of the equivalent refractive index of the unit cell with the frequency variation is shown in the Fig. 3 by using formula (1) to (3). It can be seen that the refractive index remains almost constant in the ultrawide band with different h. At 15GHz, when the height of pin changes from 0.5 mm to 1.7 mm, the equivalent refractive index ranges from 1 to 1.41, which satisfies the design parameters of a Luneburg lens. In addition, the higher the height of the pin is, the greater the refractive index of the unit becomes. In other words, we can use this unit cell to realize a wideband low-profile Luneburg lens antenna.

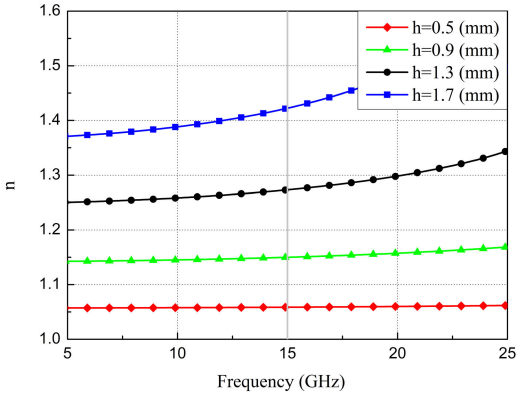

FIGURE 3. Equivalent refractive index of the glided symmetrical half-height pin under periodic conditions, as a function of the frequency for different values of the height of the pins. In both cases, the dimensions of the unit cell are $p = 4$ mm, $a = 2$ mm, and $g = 1.52$ mm.

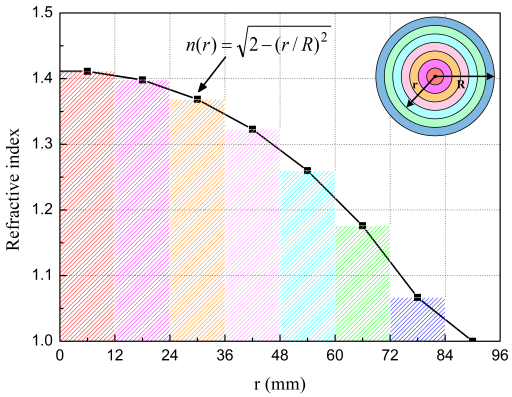

FIGURE 4. The refractive-index distribution along the radius of the Luneburg lens.

III. LOW-PROFILE LUNEBURG LENS DESIGN AND SIMULATION

The Luneburg lens is a GRIN quasi-optical devices with extremely interesting features for beamforming networks (BFN), such as axial symmetry, inducing performance independence from the excitation position, and with a good matching to the free space radiation due to a refractive index equal to 1 at the lens edge. Its main characteristic is that at any focus on the surface of the lens, it can transform the spherical wave to a plane wave at the opposite side.

A two-dimensional Luneburg lens of radius R has been designed to provide the requested index profile [37]

$$n(r) = \sqrt{2 - (r/R)^2}). \tag{4}$$

where r is the distance between a point of the lens and the center of the lens. At the center, the refractive index is equal to $\sqrt{2}$, and it ends at the edges with a refractive index equal to 1.

Next, we discretize the flat Luneburg lens into a multilayer concentric ring region. To obtain perfect lens performance, we can increase the number of layers to make the refractive index distribution much closer to the ideal Luneburg lens. Here, the flat Luneburg lens is divided into seven regions

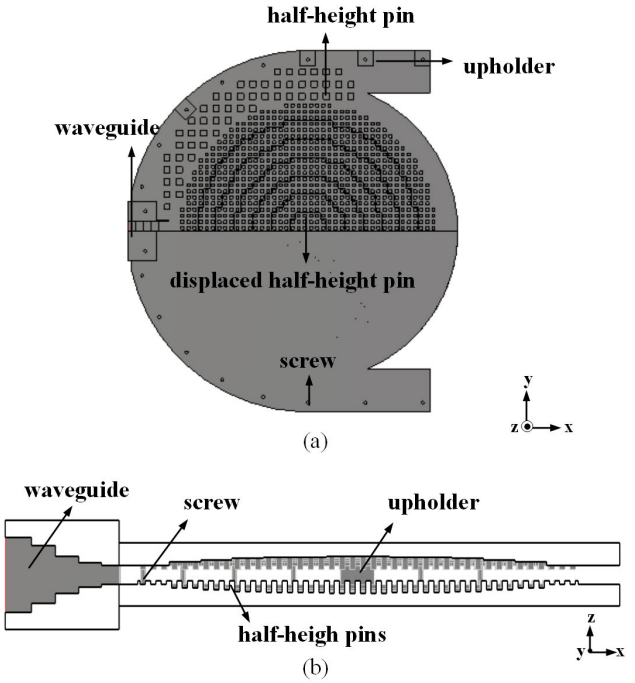

FIGURE 5. Geometry of the lens antenna. (a)Top view. (b) Side view.

TABLE 1. Refractive indices in the different regions.

layer	1	2	3	4	5	6	7
n	1.41	1.04	1.37	1.32	1.26	1.18	1.07
$h(mm)$	1.70	1.65	1.59	1.47	1.21	1.00	0.50

along its radius, and the refractive index distribution is shown in Fig. 4. Table 1 gives the variations of the refractive indices and the pin height h in different regions.

At this point, we have designed the main part of a low-profile Luneburg lens by using periodic glided half-height pins. Next, for the feed, the lens antenna is excited by a staircase waveguide for good matching. Here, we choose standard waveguide WR-51 as the feed source that operates from 14 GHz to 22 GHz. Fig. 5 shows the geometry of the antenna, which consists of a feed source, lens, upholder and screws. The staircase waveguide is placed on the focal point of the Luneburg lens. Usually, by increasing the number of stairs, the impedance matching of the proposed antenna is significantly improved. Here, we use four stairs to acquire a good impedance matching over a wide operating band. An upholder and screws are used to ensure that the air gap height between the two metal plates with half-height pins is unchanged. The screw is placed around the edge of the lens, except at the radiation direction of the lens; otherwise, it will influence the radiation characteristics. To obtain the lower back lobe, we use three rows of EBG characteristic units of a non-glided half-height pin structure arranged around the central lens, as shown in Fig.5.

The proposed antenna is optimized with the help of an electromagnetic (EM) simulator in CST Microwave Studio. The electric fields are extracted in the middle of the air gap and are given in Fig. 6. We can clearly see that the lens antenna transforms the incident spherical wave radiation into a plane wave radiation over different frequencies. From Fig.3 we can conclude that the refractive index of the unit cell will grow with increasing frequency. When the required n is larger, the rising trend of the unit is more serious in the high-frequency band. Therefore, the refractive index n is higher than 1.414 in the central region of the lens at high frequencies. At 22 GHz, the refractive index n is close to 1.48, which results in a phase delay for the electromagnetic wave along the central path. Therefore, the near-field equiphase surface appears as depressed, which deteriorates the transformation from the spherical wave to the plane wave, although it can still be seen as an approximate plane wave.

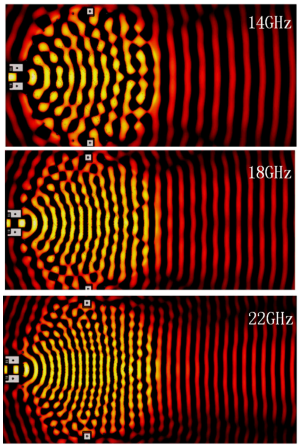

FIGURE 6. Simulated electric fields at f = 14 GHz, 18 GHz, and 22 GHz.

Fig. 7(a) presents the H-plane radiation patterns with three rows of half-height pins around the lens except in the main lobe direction used as the EBG structure, while Fig. 7(b) shows radiation patterns of the lens antenna without the EBG structure. The ϕ ranges from $-180°$ to $+180°$, when ϕ is zero, it is the boresight direciton. We can see that the back lobe is decreased with the EBG, but the sidelobe might be increased at some frequencies. As shown in Fig. 8, the computed maximum gain rises slightly with the EBG structure, especially over lower and higher frequencies, and the radiation efficiency at most frequencies is up to 60%. Here, by introducing the EBG, the energy has been prohibited from leaking from the backside of the lens and transmitting to the main lobe direction, and thus, the maximum gain and front-back ratio have been improved.

IV. ANTENNA FABRICATION AND MEASUREMENT RESULTS

To verify the antenna performance, a prototype of the lens antenna is fabricated by using CNC milling machining with aluminum. Here, we use one WR-51 standard waveguide as the feed source. Portions of the finished products are depicted in Fig. 9. The antenna is compact with a low profile, which is approximately 8 mm with a radius of 118 mm.

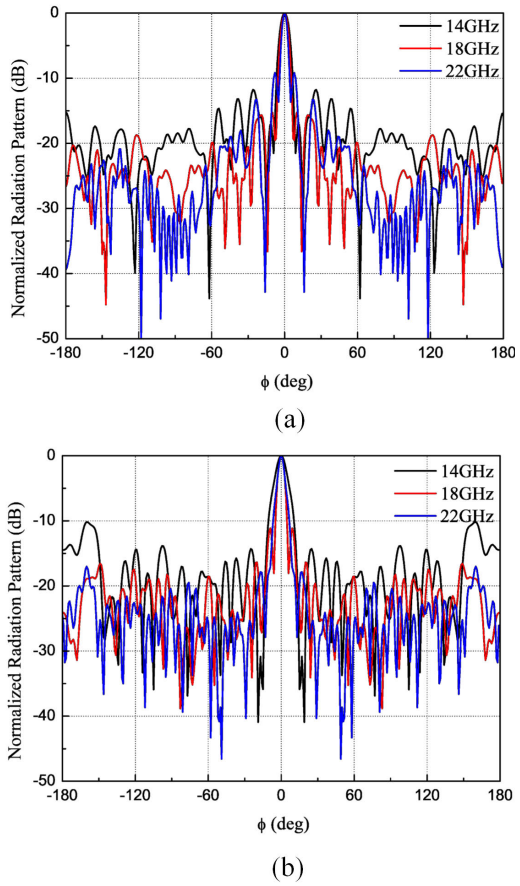

FIGURE 7. Simulated radiation patterns. (a) with three rows of half-height pins and (b) without half-height pins with three rows of a lens at different frequencies of f = 14 GHz, 18 GHz, and 22 GHz.

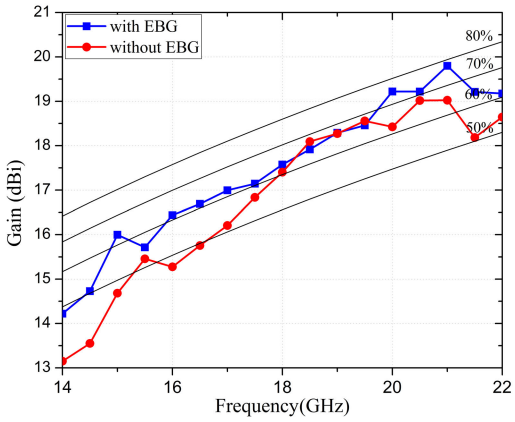

FIGURE 8. Simulated maximum gain versus the frequency range from 14 GHz to 22 GHz.

Fig. 10 shows the simulated and measured return loss and gain results. The measured return loss agrees well with the simulated return loss over most frequencies. The prototype demonstrates the return losses less than −10 dB over 14 GHz–22 GHz. However, within the frequency band of 19 GHz–20 GHz, the measured data are higher than the simulated data, which we believe is caused by the limited measurement conditions and processing error. With reference

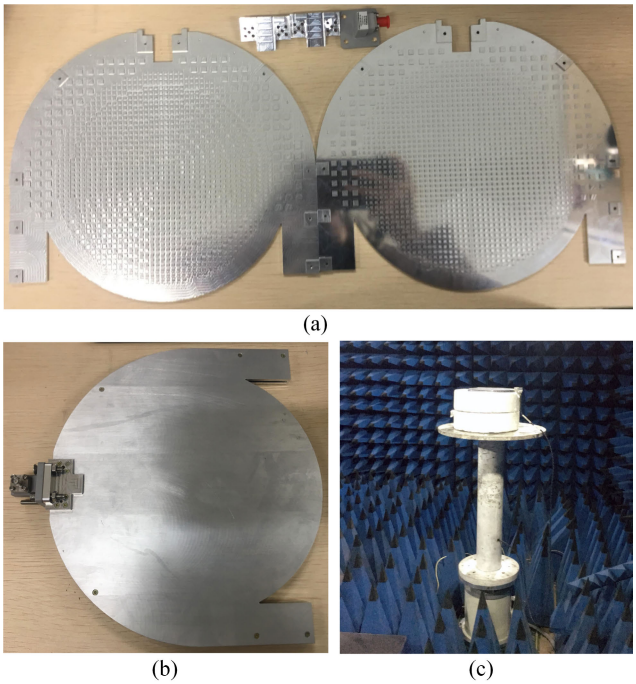

FIGURE 9. The prototype of the fabricated lens antenna. (a) The top layer, the bottom layer and staircase waveguide. (b) Lens antenna. (c) Setup of the measurement.

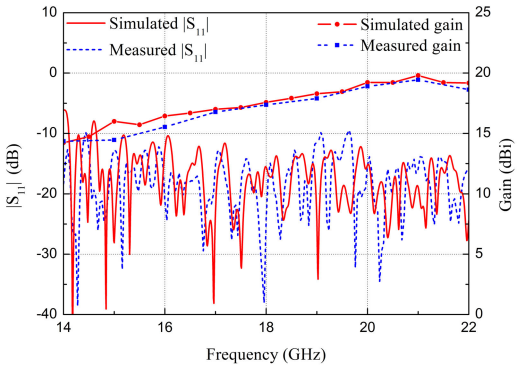

FIGURE 10. Simulated and measured return losses and gain of the antenna.

to the gain curves, we can see that the measured gain is slightly lower than the simulated gain, and the maximum gain ranges from 14.2 dBi to 19.5 dBi, which is due to the fabrication error. Fig. 11 shows the measured and simulated normalized radiation patterns at 14 GHz, 18 GHz and 22 GHz, respectively. The proposed antenna shows stable radiation performance with a half-power beamwidth of approximately 5°–8° over the entire working frequency band. Small disparities with simulated results are observed around the sidelobe level (SLL), and the measured SLL in the H-plane is approximately 3dB higher than the simulated SLL, which is attributed to the field leakage from the absorbers in the experimental setup and the disturbance from the experimental environment. However, it can be seen from the measurement results that the antenna's SLL is lower than −10 dB at most frequency points.

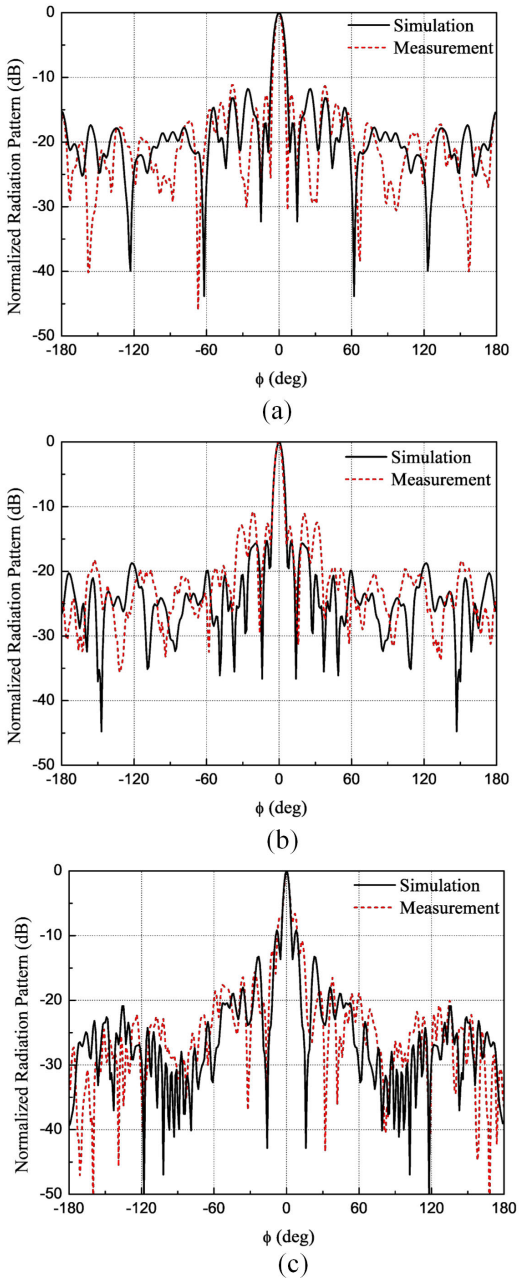

FIGURE 11. Simulated and measured H-plane radiation pattern of the lens antenna. (a)14GHz. (b)18GHz. (c)22GHz.

Finally, a characteristic comparison of the flat lenses designed by different approaches is summarized in Table 2. Literature [18] presented a non-uniform metasurface Luneburg lens using an array of circular patches with varying sizes on a dielectric substrate inside a PPW structure variable surface impedance. Literature [19] used microstrip crossed segments on PCBs, which is a kind of metamaterial, and Literature [20] proposed an all-metal lens antenna based on a variable PPW Fakir bed of nails. However, the above designs did not show the fabricated results, the correctness and accuracy of the design would not be verified. In [27], a fully glide-symmetric metallic Luneburg lens operating at the Ka-band was presented and fabricated. Here, we also have manufactured the lens and have the measured performance as seen in Table 2. Compared to these lens antennas, the proposed flat Luneburg lens antenna is compact, low-cost and low-profile, while achieving good performance in the wideband.

TABLE 2. Comparison of flat lenses designed with different approaches.

Ref.	Cent.Freq. (GHz)	Diameter (mm)	Thickness (mm)	Bandwidth	Gain@freq (dBi)(GHz)
[18]	13	151	5.75	20%	12@13
[19]	11	286	10	35%	15.9@9 18.3@12
[20]	12.5	250	10	40%	22@12.5 (directivity)
[27]	28	-	6.36	29%	18@28
This work	15	236	8	44%	14.2@14 19.5@22

V. CONCLUSION

In this paper, an effective low-profile wideband lens antenna is designed by using glided half-height pins. This antenna contains a two-layer structure that is glided a half period of the half-height pins. By adjusting the pin height of seven regions, the refractive index of the unit cell varies from 1 to 1.41. From the simulated and measured results, the performances of the lens antenna are remarkable. The lens produces a highly directive beam that has a value of approximately 14.2 dBi at 14 GHz. The gain increases up to 19.5 dBi at 22 GHz. Furthermore, the antenna is completely made of metal, and thus, low-cost metal fabrication and mass production are possible. To realize the ultrawideband application, the lens can also be designed with multiple feeds and wideband feeds.

REFERENCES

[1] A. N. Plastikov, "A high-gain multibeam bifocal reflector antenna with 40° field of view for satellite ground station applications," *IEEE Trans. Antennas Propag.*, vol. 64, no. 7, pp. 3251–3254, Jul. 2016.

[2] M. Li and K.-M. Luk, "Low-cost wideband microstrip antenna array for 60-GHz applications," *IEEE Trans. Antennas Propag.*, vol. 62, no. 6, pp. 3012–3018, Jun. 2014.

[3] N.-W. Liu, L. Zhu, W.-W. Choi, and X. Zhang, "A low-profile aperture-coupled microstrip antenna with enhanced bandwidth under dual resonance," *IEEE Trans. Antennas Propag.*, vol. 65, no. 3, pp. 1055–1062, Mar. 2017.

[4] N. Liu, L. Zhu, and W. Choi, "A Differential-fed microstrip patch antenna with bandwidth enhancement under operation of TM10 and TM30 modes," *IEEE Trans. Antennas Propag.*, vol. 65, no. 4, pp. 1607–1614, Apr. 2017.

[5] Y. Cai, Y. Zhang, H. Chen, N. Jing, Z. Qian, and S. Shi, "Design of dual circularly polarized substrate integrated waveguide horn antenna," in *Proc. IEEE Int. Conf. Microw. Millim. Wave Technol. (ICMMT)*, Beijing, China, Jun. 2016, pp. 603–605.

[6] G.-L. Huang, S.-G. Zhou, T.-H. Chio, H.-T. Hui, and T.-S. Yeo, "A low profile and low sidelobe wideband slot antenna array feb by an amplitude-tapering waveguide feed-network," *IEEE Trans. Antennas Propag.*, vol. 63, no. 1, pp. 419–423, Jan. 2015.

[7] M. Bozzi, A. Georgiadis, and K. Wu, "Review of substrate-integrated waveguide circuits and antennas," *IET Microw., Antennas Propag.*, vol. 5, no. 8, pp. 909–920, 2011.

[8] M. Ferrando-Rocher, J. I. Herranz-Herruzo, A. Valero-Nogueira, and A. Vila-Jimenez, "Single-layer circularly-polarized *Ka* -band antenna using gap waveguide technology," *IEEE Trans. Antennas Propag.*, vol. 66, no. 8, pp. 3837–3845, Aug. 2018.

[9] I. Kadri, A. Petosa, and L. Roy, "Ka-band Fresnel lens antenna fed with an active linear microstrip patch array," *IEEE Trans. Antennas Propag.*, vol. 53, no. 12, pp. 4175–4178, Dec. 2005.
[10] C. Mateo-Segura, A. Dyke, H. Dyke, S. Haq, and Y. Hao, "Flat Luneburg lens via transformation optics for directive antenna applications," *IEEE Trans. Antennas Propag.*, vol. 62, no. 4, pp. 1945–1953, Apr. 2014.
[11] H.-T. Chou and Z.-D. Yan, "Parallel-plate Luneburg lens antenna for broadband multibeam radiation at millimeter-wave frequencies with design optimization," *IEEE Trans. Antennas Propag.*, vol. 66, no. 11, pp. 5794–5804, Nov. 2018.
[12] A. Petosa and A. Ittipiboon, "Design and performance of a perforated dielectric Fresnel lens," *IEE Proc.-Microw., Antennas Propag.*, vol. 150, no. 5, pp. 309–314, 2003.
[13] K. Sato and H. Ujiie, "A plate Luneberg lens with the permittivity distribution controlled by hole density," *Electron. Commun. Jpn. (Part I, Commun.)*, vol. 85, no. 9, pp. 1–12, Sep. 2002.
[14] A. O. Diallo, R. Czarny, B. Loiseaux, and S. Hole, "Comparison between a thin lens antenna made of structured dielectric material and conventional lens antennas, in Q-band in a compact volume," *IEEE Antennas Wireless Propag. Lett.*, vol. 17, no. 2, pp. 307–310, Feb. 2018.
[15] C. D. Diallo, O. Quevedo-Teruel, G. Valerio, H. Legay, and R. Sauleau, "Parallel-plate-waveguide Luneburg lens through a holey plate metasurface," in *Proc. 9th Eur. Conf. Antennas Propag. (EuCAP)*, Lisbon, Portugal, Apr. 2015, pp. 1–2.
[16] A. Dhouibi, S. N. Burokur, and A. de Lustrac, "Planar metamaterial-based beam-scanning broadband microwave antenna," *J. Appl. Phys.*, vol. 115, no. 19, May 2014, Art. no. 194901.
[17] Q. Cheng, H. F. Ma, and T. J. Cui, "Broadband planar Luneburg lens based on complementary metamaterials," *Appl. Phys. Lett.*, vol. 95, no. 18, Nov. 2009, Art. no. 181901.
[18] M. Bosiljevac, M. Casaletti, F. Caminita, Z. Sipus, and S. Maci, "Non-uniform metasurface Luneburg lens antenna design," *IEEE Trans. Antennas Propag.*, vol. 60, no. 9, pp. 4065–4073, Sep. 2012.
[19] C. Pfeiffer and A. Grbic, "A printed, broadband Luneburg lens antenna," *IEEE Trans. Antennas Propag.*, vol. 58, no. 9, pp. 3055–3059, Sep. 2010.
[20] C. D. Diallo, E. Girard, H. Legay, and R. Sauleau, "All-metal ku-band Luneburg lens antenna based on variable parallel plate spacing fakir bed of nails," in *Proc. 11th Eur. Conf. Antennas Propag. (EUCAP)*, Paris, France, Mar. 2017, pp. 1401–1404.
[21] R. Mittra and S. Laxpati, "Propagation in a wave guide with glide reflection symmetry," *Can. J. Phys.*, vol. 43, pp. 353–372, Feb. 1965.
[22] R. Kieburtz and J. Impagliazzo, "Multimode propagation on radiating traveling-wave structures with glide-symmetric excitation," *IEEE Trans. Antennas Propag.*, vol. AP-18, no. 1, pp. 3–7, Jan. 1970.
[23] P. J. Crepeau and P. R. McIsaac, "Consequences of symmetry in periodic structures," *Proc. IEEE*, vol. 52, no. 1, pp. 33–43, Jan. 1964.
[24] M. Ebrahimpouri, E. Rajo-Iglesias, Z. Sipus, and O. Quevedo-Teruel, "Cost-effective gap waveguide technology based on glide-symmetric holey EBG structures," *IEEE Trans. Microw. Theory Techn.*, vol. 66, no. 2, pp. 927–934, Feb. 2018.
[25] E. Rajo-Iglesias, M. Ebrahimpouri, and O. Quevedo-Teruel, "Wideband phase shifter in groove gap waveguide technology implemented with glide-symmetric holey EBG," *IEEE Microw. Wireless Compon. Lett.*, vol. 28, no. 6, pp. 476–478, Jun. 2018.
[26] O. Quevedo-Teruel, M. Ebrahimpouri, and M. N. M. Kehn, "Ultrawideband metasurface lenses based on off-shifted opposite layers," *IEEE Antennas Wireless Propag. Lett.*, vol. 15, pp. 484–487, Dec. 2016.
[27] O. Quevedo-Teruel, J. Miao, M. Mattsson, A. Algaba-Brazalez, M. Johansson, and L. Manholm, "Glide-symmetric fully metallic Luneburg lens for 5G communications at Ka-band," *IEEE Antennas Wireless Propag. Lett.*, vol. 17, no. 9, pp. 1588–1592, Sep. 2018.
[28] M. Ebrahimpouri and O. Quevedo-Teruel, "Ultrawideband anisotropic glide-symmetric metasurfaces," *IEEE Antennas Wireless Propag. Lett.*, vol. 18, no. 8, pp. 1547–1551, Aug. 2019.
[29] J. Zhang, F. Fan, and J. Wu, "Ultra wide band lens antenna based on periodic displaced symmetry half-height pins," in *Proc. Int. Conf. Microw. Millim. Wave Technol. (ICMMT)*, Chengdu, China, May 2018, pp. 1–3.
[30] E. Rajo-Iglesias and P.-S. Kildal, "Numerical studies of bandwidth of parallel-plate cut-off realised by a bed of nails, corrugations and mushroom-type electromagnetic bandgap for use in gap waveguides," *IET Microw., Antennas Propag.*, vol. 5, no. 3, pp. 282–289, 2011.
[31] F. Fan, J. Yang, V. Vassilev, and A. U. Zaman, "Bandwidth investigation on half-height pin in ridge gap waveguide," *IEEE Trans. Microw. Theory Techn.*, vol. 66, no. 1, pp. 100–108, Jan. 2018.
[32] N. Memeletzoglou, C. Sanchez-Cabello, F. Pizarro-Torres, and E. Rajo-Iglesias, "Analysis of periodic structures made of pins inside a parallel plate waveguide," *Symmetry*, vol. 11, no. 4, p. 582, 2019.
[33] P.-S. Kildal, A. U. Zaman, E. Rajo-Iglesias, E. Alfonso, and A. Valero-Nogueira, "Design and experimental verification of ridge gap waveguide in bed of nails for parallel-plate mode suppression," *IET Microw., Antennas Propag.*, vol. 5, no. 3, pp. 262–270, 2011.
[34] E. Rajo-Iglesias and P.-S. Kildal, "Groove gap waveguide: A rectangular waveguide between contactless metal plates enabled by parallel-plate cut-off," in *Proc. 4th Eur. Conf. Antennas Propag. (EuCAP)*, Barcelona, Spain, Apr. 2010, pp. 1–4.
[35] E. Pucci, A. U. Zaman, E. Rajo-Iglesias, and P.-S. Kildal, "New low loss inverted microstrip line using gap waveguide technology for slot antenna applications," in *Proc. 5th Eur. Conf. Antennas Propag. (EuCAP)*, Rome, Italy, Apr. 2011, pp. 979–982.
[36] D. R. Smith, D. C. Vier, T. Koschny, and C. M. Soukoulis, "Electromagnetic parameter retrieval from inhomogeneous metamaterials," *Phys. Rev. E, Stat. Phys. Plasmas Fluids Relat. Interdiscip. Top.*, vol. 71, no. 3, Mar. 2005, Art. no. 036617.
[37] R. K. Luneburg and M. Herzberger, *Mathematical Theory of Optics*. Berkeley, CA, USA: Univ. of California Press, 1964.

FANGFANG FAN (Member, IEEE) was born in Xianyang, Shaanxi, China. She received the B.S. degree from Xidian University, Xi'an, China, in 2003, the M.E. degree in electromagnetic field and microwave technology from the University of Electronic Science and Technology of China, in 2006, and the Ph.D. degree in electromagnetic field and microwave technology from Xidian University, in 2011. Since 2006, she has been working with Xidian University. From March 2015 to March 2016, she was a Visiting Scholar with the Chalmers University of Technology, Sweden. She is currently an Associate Professor with the National Key Laboratory of Antennas and Microwave Technology, Xidian University. Her research interests include broadband and miniaturization antenna design, and gap waveguide technology and its application in antenna.

MINGBO CAI was born in Xianyang, Shaanxi, China, in 1993. He received the B.S. degree in electronic and information engineering from Chang'an University, Xi'an, China, in 2011. He is currently pursuing the Ph.D. degree in electromagnetic field and microwave technology with Xidian University, Xi'an. His research interests include microstrip antenna arrays, reflector antenna, reflectarray antenna, and transmitarray antenna.

JIACHEN ZHANG was born in Datong, Shanxi, China, in 1994. She received the B.S. degree from the Taiyuan University of Technology, Taiyuan, China, in 2016, and the M.E. degree in electromagnetic field and microwave technology from Xidian University, Xi'an, China, in 2019. Her research interests include waveguide slot antenna, gap waveguide, and lens antenna.

ZEHONG YAN was born in Tianmen, Hubei, China, in 1964. He received the B.S. and M.E. degrees in electromagnetic field and microwave technology from Xidian University, Xi'an, China, in 1980 and 1984, respectively, and the Ph.D. degree from Northwestern Polytechnical University, Xi'an, in 1996. He joined Xidian University, in 1984, where he is currently a Professor with the School of Electronic Engineering. His research interests include communications antenna, antenna tracking technology, and microwave device.

JINXIAO WU was born in Xi'an, Shaanxi, China, in 1992. He received the B.S. degree in electromagnetic field and microwave technology from the Xi'an University of Telecommunications, Xi'an, China, in 2012, and the M.E. degree in electromagnetic field and microwave technology from Xidian University, Xi'an, in 2019. His research interests include planar antenna, microstrip antenna arrays, and gap waveguide.